Journal of Applied Physics

Ionoluminescence and optical transmission investigation of ZnO(In) fast ceramic scintillator irradiated with swift heavy ions

Cite as: J. Appl. Phys. **132**, 195901 (2022); https://doi.org/10.1063/5.0110205
Submitted: 15 July 2022 • Accepted: 25 October 2022 • Published Online: 15 November 2022

Maxim Saifulin, Plamen Boutachkov, Elena Gorokhova, et al.

Journal of Applied Physics ARTICLE scitation.org/journal/jap

Ionoluminescence and optical transmission investigation of ZnO(In) fast ceramic scintillator irradiated with swift heavy ions

Cite as: J. Appl. Phys. **132**, 195901 (2022); doi: 10.1063/5.0110205
Submitted: 15 July 2022 · Accepted: 25 October 2022 ·
Published Online: 15 November 2022

Maxim Saifulin,[1,2,a)] Plamen Boutachkov,[1] Elena Gorokhova,[3] Piotr Rodnyi,[4] Pascal Simon,[5,b)] Christina Trautmann,[1,2] Ivan Venevtsev,[4] and Beata Walasek-Höhne[1]

AFFILIATIONS

[1]GSI Helmholtz Center for Heavy Ion Research, Darmstadt 64291, Germany
[2]Technical University Darmstadt, Darmstadt 64289, Germany
[3]Joint Stock Company "Research and Production Corporation S.I. Vavilova," St. Petersburg 192171, Russia
[4]Peter the Great Polytechnic University, St. Petersburg 195251, Russia
[5]CERN, Geneva 1211, Switzerland

Note: The results presented in this paper are based on work performed before February 24, 2022.
[a)]**Author to whom correspondence should be addressed:** M.Saifulin@gsi.de
[b)]This research was performed while P. Simon was at GSI Helmholtz Center for Heavy Ion Research, Darmstadt, 64291, Germany and Technical University Darmstadt, Darmstadt, 64289, Germany.

ABSTRACT

Indium doped zinc oxide, ZnO(In), is a promising scintillation material for nanosecond-fast beam monitoring and counting heavy ions of MeV energy and above. We investigated the ionoluminescence and UV/Vis light transmission spectra that occur in ZnO(In) ceramic exposed to 4.8 MeV/u ^{48}Ca and ^{197}Au ions up to 5×10^{12} and 2×10^{11} ions/cm^2, respectively. Ionoluminescence and UV/Vis light transmission spectra were measured online as a function of fluence. Ionoluminescence is characterized by an intensive single emission band at 387 nm due to near-band-edge emission. We observed that the loss of the ionoluminescence intensity is more sensitive to the ion-beam-induced radiation damage than the loss of the optical transmission. The ionoluminescence intensity reduction as a function of ion fluence is described within the Birks–Black model. ZnO(In) exhibits higher radiation hardness and, thus, a longer lifetime than plastic scintillators used so far for fast-counting applications.

I. INTRODUCTION

The measurement of the absolute beam intensity and the characterization of the time structure of particle beams are standard in all particle accelerator facilities worldwide. At the GSI accelerator facility (Darmstadt, Germany),[1] where beams from protons up to uranium are accelerated and extracted from the SIS18 synchrotron at energies above 150 MeV/u, scintillation counters are routinely used as a part of particle detector combinations usually including scintillation counter, ionization chamber, and secondary electron monitor.[2,3] Scintillation counters are inserted directly into the ion beam, and each particle passed through the detector's active area creates a light pulse registered via a photo-multiplier tube (PMT). As a result, scintillation counters provide a robust, systematic-error-free way to measure accelerated particle beam currents, as each particle corresponds to a separate PMT signal that is analyzed.

Plastic scintillators are the most common choice for scintillation detector applications. They exhibit high light output, leading to high detector signal amplitudes and clear signal discrimination. Moreover, plastics show short scintillation decay times that lead to short signal widths and low signal pileup probability. Also, they are low-cost and can be produced in various sizes and shapes. However, radiation hardness remains the weakest point of plastic

scintillators. As a result of radiation damage created by heavy ions, the amount of light emitted from the plastic scintillator quickly reduces. When the detector signals become too weak to be detected by a discriminator, plastic scintillators must be exchanged, leading to a loss of valuable experimental beam time.

Searching for new radiation-hard scintillator alternatives to plastic scintillators is in demand. The candidate scintillators for fast counting of high-energy ions should exhibit fast scintillation in the nanosecond time range, be mechanically and chemically stable, and have a high tolerance to ion radiation.

Previously, materials such as GSO(Ce), YAP(Ce), CsI(pure), ZnO(In), and ZnO(Ga) have been studied as promising scintillators for fast heavy-ion counting.[4–7] In this study, we explore ZnO-based scintillators in more detail because they exhibit the shortest decay time (<1 ns) compared to other inorganic scintillators mentioned above.

ZnO has attracted scientific interest as a promising fast scintillating material for ionizing particle detection applications since the 1960s.[8,9] Two luminescence bands are distinguished in pure zinc oxide.[10] The first band is characterized by an ultra-fast luminescence with a decay time below 1 ns. It is a short-wavelength band with an exciton nature situated close to the material absorption edge (so-called near-band-edge emission, NBE). The decay time of the second band is in the order of milliseconds. The band is rather broad and comes from native defects present in the material. Its maximum intensity is around the green light spectral region (frequently referred to in the literature as deep-level emission, DL). It has been shown that impurities in ZnO, such as In, Ga, and Al, can significantly enhance NBE relative to DL emission depending on impurity concentrations. This allows ZnO to provide the fastest luminescence response time of all known inorganic scintillators.[6,11–20]

There have been several attempts to use ZnO in the form of powders, nanostructures, thin layers, single crystals, and ceramics to build x-ray, neutron, proton, and alpha-particle detectors for medical, industrial, and scientific purposes.[12,21–26] Recently, ZnO was used for the first time to detect relativistic heavy ions.[7] Despite the high interest in ZnO for radiation detector application, there is limited information on ZnO radiation hardness. Radiation hardness becomes especially critical when the detection of heavy ions is considered.

High radiation resistance of ZnO has been reported previously for single- and poly-crystals, nanostructures, and NiO/ZnO heterojunctions irradiated with protons and heavy ions.[27–34] These studies mainly focused on electric, structural, and optical properties for electronics and solar-cell applications in space. Regarding the light emission properties, one can note the work of Koike *et al.*,[28] where room temperature photoluminescence of ZnO thin films and bulk single crystals was studied as a function of fluence with 8 MeV protons. The photoluminescence (PL) intensity remained nearly unchanged up to 2×10^{12} protons/cm^2 for the ZnO bulk crystal, and 5×10^{14} protons/cm^2 for thin film samples. The reduction in PL was investigated up to a fluence of 10^{17} protons/cm^2. It was predominantly NBE emission observed without developing a significant DL emission. In the work by Pal *et al.*,[30] the formation of a new sub-bandgap absorption band around 407 nm was observed for ZnO single crystals irradiated with 700 keV ^{16}O at a fluence of 3×10^{15} ions/cm^2. This absorption band was associated with neutral oxygen vacancies and was responsible for ZnO's red-brown coloration after irradiation. Recent studies by Gupta *et al.*[35] and Singh *et al.*[36] show that energetic heavy-ion irradiation leads to suppression of NBE and enhancement of DL emission as observed in ZnO thin films with the PL method.

Ionoluminescence (IL) of ZnO(In) and ZnO(Ga) ceramics has been previously studied as a function of radiation dose by Boutachkov *et al.*[7] using 300 MeV/u ^{124}Xe and ^{238}U ions. For both materials, the IL intensity decreased by 75% of the initial intensity, reaching an absorbed dose of 4 MGy, which corresponds to approximately 10^{12} U − ions/cm^2.

Further studies are required to understand in more detail how ZnO ionoluminescence spectra change at very high radiation doses. It remains unclear whether the ionoluminescence intensity reduction is due to the loss of the light transmission and if new luminescence bands are formed.

In this study, we investigate the performance of ZnO(In) scintillating ceramics for application as a fast counter for heavy ions, with a particular focus on changes in ionoluminescence and optical transmission as a function of fluence. Ionoluminescence and UV/Vis light transmission spectra were measured online and *in situ*, during beam stops, respectively. Swift heavy ions with an energy of 4.8 MeV/u were used. At this specific energy, the stopping power and the deposited energy density are maximum; thus, the accumulation of doses above 4 MGy can be reached in a shorter time than for 300 MeV/u ion beams.

II. MATERIALS AND METHODS

A. Samples

Indium doped zinc oxide, ZnO(In), ceramic samples with 0.046 at% In^{3+} doping concentration were produced by Joint Stock Company "Research and Production Corporation S.I. Vavilova" (St. Petersburg, Russia) using a hot uni-axial pressing technique in vacuum with a successive thermal treatment in (H_2/Ar) atmosphere. Additional information about the sample fabrication can be found in Refs. 14 and 15. Samples were translucent and had a rough surface finishing, $R_a = (8.1 \pm 1.5)\mu$m. The sample plates were 0.4 mm thick and had a size of approximately 8×8 mm^2.

B. Irradiation procedure

The samples were irradiated with 4.8 MeV/u $^{48}Ca^{10+}$ and $^{197}Au^{26+}$ pulsed ion beams delivered by the UNIversal Linear Accelerator (UNILAC) at GSI.[37] The pulse duration was 5 ms, with a repetition rate of 2.6 and 25 Hz for the Ca and Au ions, respectively. The beam was defocused and cut by a system of slits, providing homogeneous irradiation of the sample surface. The average beam flux during the irradiation was between 10^8 and 10^9 ions/(cm^2 s) preventing macroscopic sample heating. A maximum ion fluence of 5×10^{12} and 2×10^{11} ions/cm^2 was reached for the Ca and Au ions, respectively. The irradiation was performed at a beam incidence of 45° with respect to the sample surface. All irradiations were performed at room temperature in vacuum.

The SRIM-2013 code[38] was used to calculate the ion penetration depth and stopping power depth profiles (see Fig. 1). For the

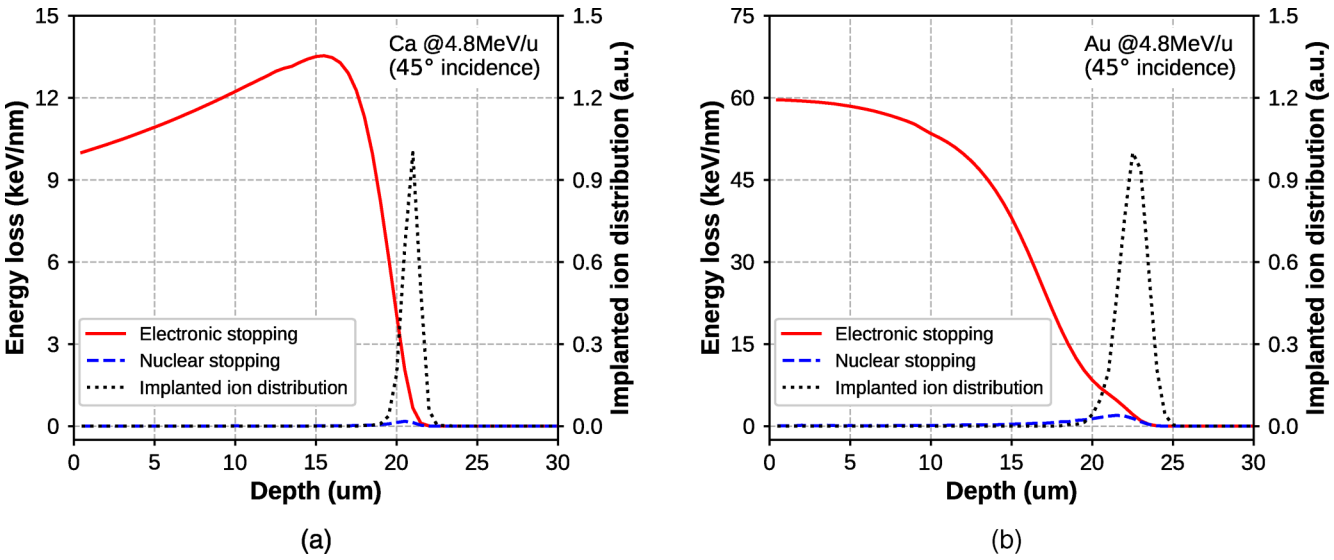

FIG. 1. SRIM-2013 calculated electronic and nuclear stopping powers, and implanted ion depth profiles for 4.8 MeV/u ^{48}Ca (a) and ^{197}Au ions (b) in ZnO at 45° beam incidence angle.

SRIM-2013 calculations, a density of 5.6 g/cm^3 was assumed, like for pure ZnO single crystal. For both ion species, the energy loss is dominated by electronic stopping down to a few micrometers before the ions stop. The calculated penetration depth under 45° beam incidence is (20.7 ± 0.6) and $(22.6 \pm 0.9)\,\mu$m for Ca and Au ions, respectively. Therefore, the ion-irradiated layers are much thinner than the thickness of the samples.

A calculation with the ETACHA code[39] showed that the equilibrium charge states for both Ca and Au ions are reached within less than 200 nm below the irradiated surface. Therefore, the effects related to the ion beam charge state equilibration were neglected in calculating stopping powers and penetration depths.

C. Measurement details

Ionoluminescence spectra were recorded online during irradiation. The irradiation was interrupted at selected fluences to record UV/Vis light transmission spectra. A schematic view of the experimental setups for IL and transmission measurements is shown in Fig. 2.

The beam intensity and irradiation fluence were monitored by a system of horizontal and vertical slits [Fig. 2(a)]. The shutters of the system of slits were individually read out via charge integrators. They were calibrated compared to the charge measured with a Faraday cup (FC) placed downstream from the slits in front of the measured sample. The Faraday cup was also used for stopping the beam during the light transmission measurements [Fig. 2(b)].

The investigated sample was mounted on a target holder (T) behind a 6 mm diameter circular collimator. It defined the region of the sample exposed to the ion beam. The biconvex lens marked as L1 was used to collect light emitted from the irradiated sample region. A second lens L2, connected to a continuous light source, was placed further downstream. This lens served for the illumination of the sample during the UV/Vis transmission measurements.

Both ionoluminescence and transmission spectra were recorded with an Ocean Optics QE-Pro spectrometer. The signal-to-noise ratio was optimized via variation of the spectrum acquisition time, ranging from 1 to 5 s. Each spectrum was corrected for dark counts and normalized by the number of ions that hit the sample during the spectrum acquisition.

The incident light source for the UV/Vis transmission measurements was a Mikropac DH-2000-BAL UV/VIS/NIR equipped with deuterium and tungsten halogen lamps. It provided a continuous spectrum with a stable light intensity in a wavelength range from 210 to 2500 nm. The source was supplied with a remotely controllable shutter, which allowed us to leave the source lamps switched on during the IL measurements. The transmitted light was collected from the side of the sample exposed to the ion beam. For each selected fluence, the transmitted light spectra were recorded with an acquisition time of 10 s. The measured ten spectra were averaged for each fluence. Before the sample irradiation, a spectrum of the incident light was recorded with the empty target holder with an acquisition time of 0.5 s. All spectra were corrected for dark counts and normalized by the corresponding acquisition time. The resulting transmission spectra at different ion fluences were calculated as

$$T(\Phi, \lambda) = \frac{S_{tr}(\Phi, \lambda)}{S_{in}(\lambda)}, \quad (1)$$

where Φ is the ion fluence, λ is the light wavelength, $S_{tr}(\Phi, \lambda)$ is the spectrum of the light transmitted through the sample irradiated to the fluence Φ, and $S_{in}(\lambda)$ is the incident light spectrum. It should be noted that a part of the transmitted light was not collected by the

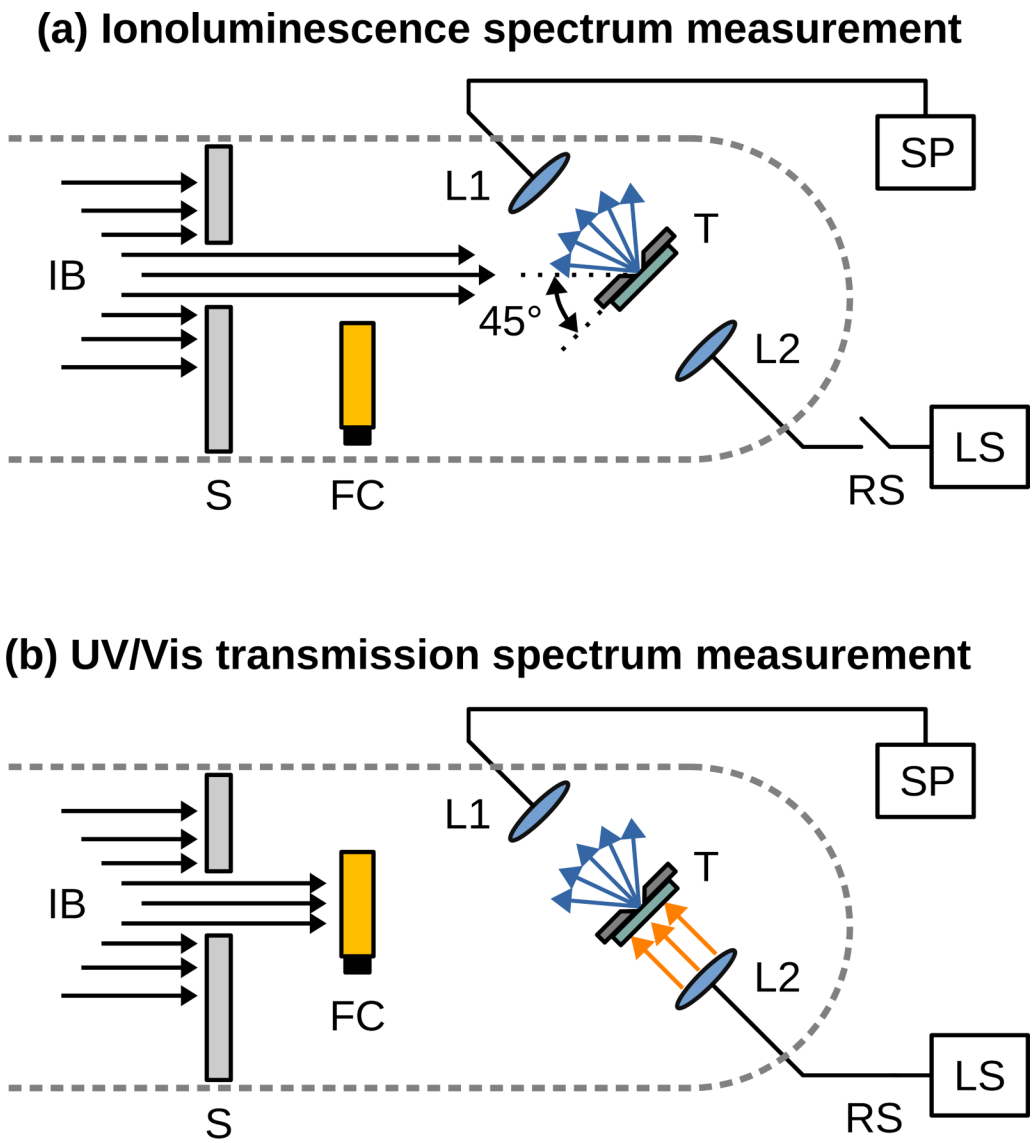

FIG. 2. Schematic view of the experimental setup. For ionoluminescence measurements (a), the Faraday cup (FC) is removed from the beam path. The luminescence light spectrum is recorded with the spectrometer (SP). Transmission measurements (b) are performed by inserting the Faraday cup to block the beam. The transmission of light from a continuous light source (LS) is quantified by the same spectrometer (SP) used in measurement (a). The dashed line indicates the walls of the vacuum chamber. IB—ion beam from the accelerator, S—slit for the ion beam collimation and on-line beam flux monitoring, T—target holder, L1 and L2—optical biconvex lenses, RS—remotely controllable shutter.

lens L1 due to diffuse light scattering. Therefore, the transmission measured in our spectrometer is smaller than the total transmission value.

The ion penetration depth in these experiments was significantly shorter than the thickness of the sample. The sample layer, which is deeper than the ion penetration depth, remains non-irradiated. It is assumed that the transmission of the non-irradiated layer of the sample does not change with fluence. The measured transmission can be split into two parts as follows:

$$T(\Phi, \lambda) = T_{\mathrm{irr}}(\Phi, \lambda) \times T_{\mathrm{prist}}(\lambda), \tag{2}$$

where $T_{\mathrm{irr}}(\Phi, \lambda)$ is the transmission through the irradiated layer and $T_{\mathrm{prist}}(\lambda)$ is the transmission through the pristine layer.

If one considers the transmission measured for a fluence Φ, $T_{\Phi} = T(\Phi, \lambda)$, relative to the initial transmission measured before irradiation, $T_{\mathrm{init}} = T(0, \lambda)$, one can exclude $T_{\mathrm{prist}}(\lambda)$ and get the relative transmission that occurs only in the irradiated layer,

$$T_\Phi/T_{\text{init}} = T_{\text{irr}}(\Phi, \lambda)/T_{\text{irr}}(0, \lambda). \quad (3)$$

The relative comparison also applies to ionoluminescence spectra changes. In this case, the first acquired ionoluminescence spectrum at a low fluence is treated as the initial spectrum, and all further spectra are calculated relative to it. It is important to note that the initial ionoluminescence spectrum fluence is not equal to zero, since the sample must be exposed to the beam to get a spectrum. Therefore, we denote the relative ionoluminescence spectra as I_Φ/I_{init^*}, where the star indicates that the initial ionoluminescence is not at zero fluence.

III. RESULTS

A. UV/Vis light transmission

The irradiation of ZnO(In) samples with both Ca and Au ions led to a yellow-orange coloration of the irradiated region. Photos of a ZnO(In) sample before and after irradiation with Au ions up to 2×10^{11} ions/cm^2 fluence are shown in Fig. 3. The circular spot of 5 mm in diameter in the middle of the sample results from the ion beam exposure.

The transmission spectra obtained at various Ca and Au ion fluences are presented in Fig. 4. The diffuse light scattering from the sample (originating from the rough surface of the sample), together with the low light collection efficiency of the setup (due to a limited solid angle where light is collected), led to registered transmission values below 0.03%. The maximum transmission of 0.026% is observed around 550 nm wavelength for non-irradiated samples. The transmission sharply drops to zero for wavelengths below 390 nm. This drop is associated with an absorption near the band (fundamental) edge. The transmission loss observed in the long-wavelength region (>600 nm) is due to free charge carrier absorption caused by the presence of shallow donors created by the indium impurity.

As a result of the ion irradiation, the transmission in UV and visible light regions reduces by increasing the fluence for both ion species. The loss of transmission in UV and visible regions leads to a shift of the maximum transmission wavelength from 550 nm to 600 nm. We assume that the loss of transmission at short wavelengths together with the red shift of the transmission maximum is responsible for the yellow-orange coloration shown in Fig. 3. Based on previous ZnO studies, there are various explanations of what could be the reason for the yellow-orange coloration in ZnO. The majority of publications discuss the role of oxygen vacancy defects and ascribe the photon absorption in the blue region to the color change.[30,40–42] On the other hand, authors in Refs. 43 and 44 assume that zinc vacancies lead to the absorption at 420 nm.

At the same time, there is no significant change in the IR region for wavelengths above 600 nm (irradiation with Ca ions) and above 700 nm (irradiation with Au ions). As previously reported by Chernenko *et al.*,[15] the absorption at long wavelengths in ZnO(In) ceramics depends on the free charge carrier concentration. Since none of the irradiated samples show a change in transmission above 600 nm (Ca ions) or 700 nm (Au ions), this may indicate that the ion irradiation does not change the effective charge carrier concentration within the investigated fluence ranges.

B. Ionoluminescence spectra

Figure 5 shows the ionoluminescence spectra of ZnO(In) samples irradiated at various fluences with 4.8 MeV/u Ca and Au ions. The initial IL spectra were recorded at a low fluence of 6×10^9 Ca $-$ ions/cm^2 and 4×10^8 Au $-$ ions/cm^2. For both ion species, the initial IL spectra show a single emission band in the UV light region at ~387 nm. This band is ascribed to the near-band-edge emission and was also observed in a previous study from Boutachkov *et al.*,[7] where ZnO(In) ceramics were exposed to 4.8 MeV/u ^{120}Sn ions.

With increasing ion fluence, the peak position shifts from 387 to 395 nm for the Au ion irradiation up to 2×10^{11} ions/cm^2,

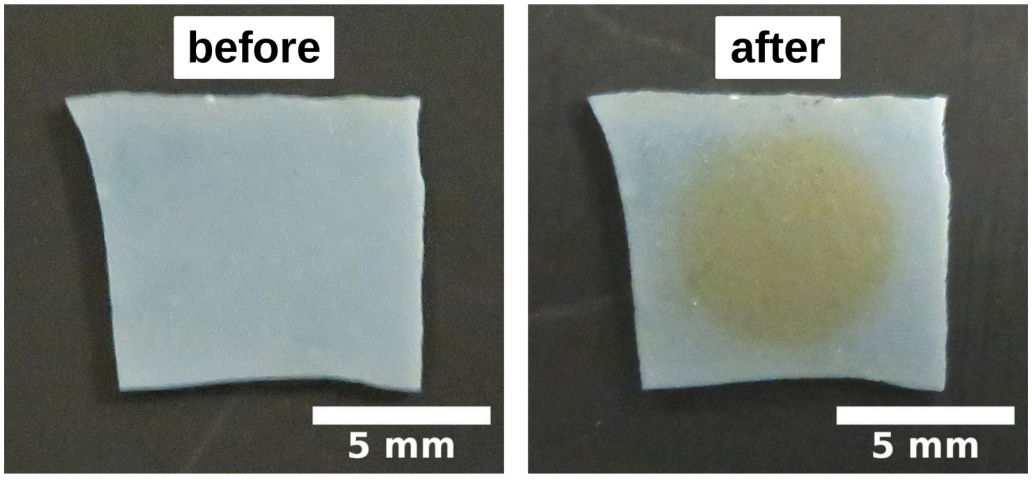

FIG. 3. ZnO(In) scintillating ceramic sample before and after 4.8 MeV/u ^{197}Au ion irradiation up to 2×10^{11} ions/cm^2.

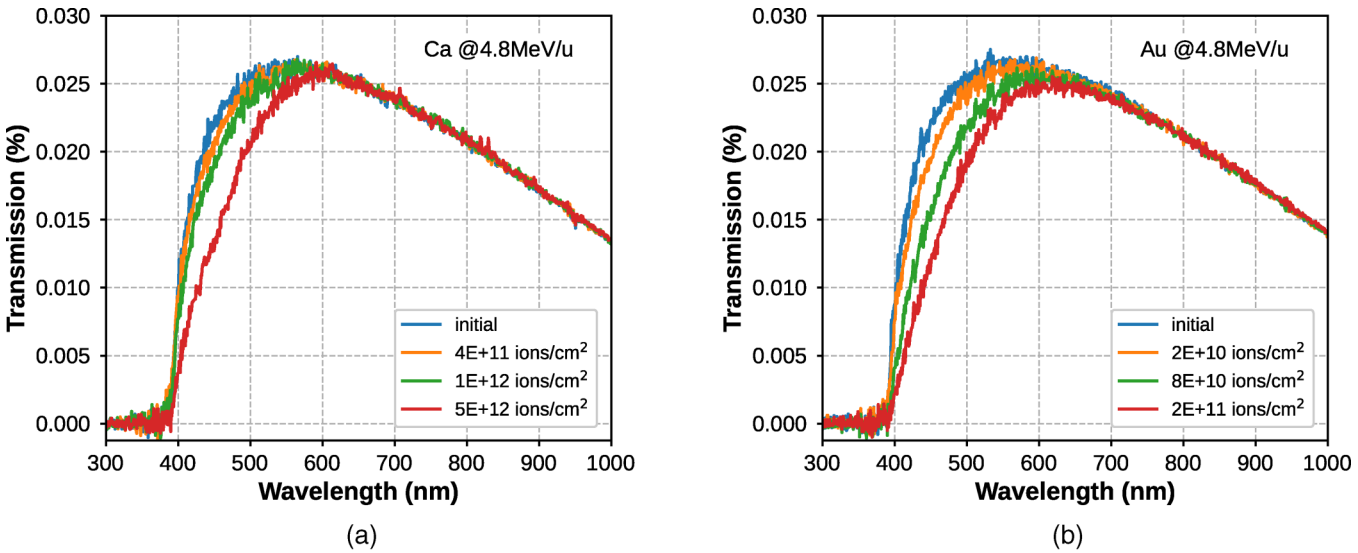

FIG. 4. Transmission spectra of ZnO(In) scintillating ceramic irradiated at various fluences with 4.8 MeV/u ^{48}Ca (a) and ^{197}Au (b) ions. The ion incidence angle with respect to the sample surface was 45°.

while for the Ca irradiation, the peak position scatters by 1–2 nm, which is within the measurement error. The NBE peak intensity drops with increasing fluence. No new peaks are formed during the irradiation, even at the highest fluences.

We note that there is a discrepancy with respect to the intensity change of DL emission as a result of heavy-ion irradiation that has been reported for photo-induced luminescence (PL), x-ray-induced luminescence (XRL), and ion-induced luminescence (IL).[19,35,36] Previous PL studies on ZnO thin films exposed to MeV Ni, Ag, and Au ions at much higher fluences than in our experiment showed an increase in DL emission.[35,36] Increase in DL emission was not observed for XRL characterization of ZnO(In) samples irradiated with relativistic U ions at 10^{12} ions/cm^2 fluence.[19] The IL results of the current work also show the absence

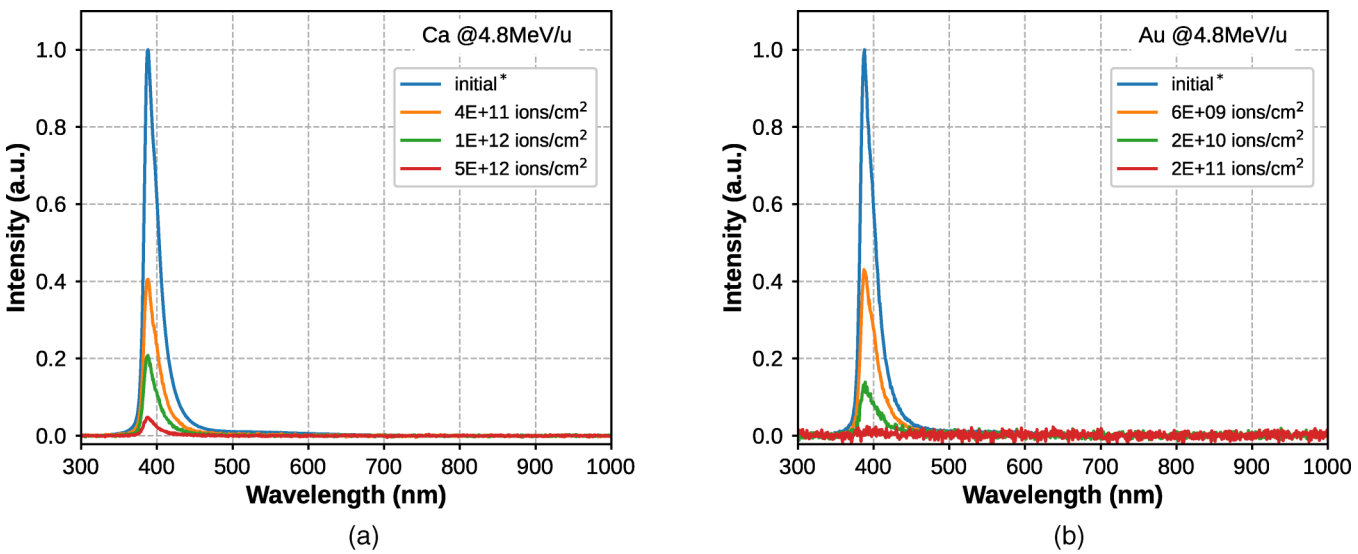

FIG. 5. Ionoluminescence spectra of ZnO(In) scintillating ceramic irradiated at various fluences with 4.8 MeV/u ^{48}Ca (a) and ^{197}Au (b) ions. The ion incidence angle with respect to the sample surface was 45°. Initial IL spectra correspond to a fluence of 6×10^9 Ca − ions/cm^2 and 4×10^8 Au − ions/cm^2, respectively.

of the DL emission growth in ZnO(In) ceramics as a result of swift Ca and Au irradiation. The fact that the slow DL emission remains negligible compared to the fast NBE emission over the entire investigated range of heavy-ion fluences is advantageous for the application as a fast scintillation counter. Further irradiation experiments in a broad range of fluences are of interest to allow a more accurate comparison of PL, XRL, and IL spectra.

IV. DISCUSSION

A. Relative ionoluminescence and transmission changes

Figures 6 and 7 show relative IL intensity and optical transmission at various fluences for samples irradiated with Ca and Au ions. Wavelength cut-offs are imposed on data used to calculate the relative ionoluminescence and transmission to exclude division by values close to zero. For both ion species, the most significant change of the relative transmission is observed just above the cut-off wavelength around 390–400 nm wavelength, being reduced by 65% of the initial transmission for the sample irradiated with 5×10^{12} Ca − ions/cm^2 and by 85% for the sample irradiated with 2×10^{11} Au − ions/cm^2. In the same spectral region, the relative IL intensity change is more pronounced than T_Φ/T_{init} dropping approximately by 95% and 99.5% of the initial IL intensity. This indicates that the IL intensity loss observed as a function of fluence is more sensitive to the beam-induced radiation damage than to the loss of light transmission.

As shown in Fig. 1, the energy deposition of both Ca and Au ions in ZnO is not homogeneous as a function of depth. It, thus, can be expected that, within the irradiated layer, the contribution to the transmission loss also varies with depth. Nevertheless, the transmission in any sub-layer from zero up to ion penetration depth cannot be larger than the transmission of the whole irradiated layer. Thus, relative transmission measurements performed in this work define the upper limit of a relative transmission change due to the Ca and Au ion irradiation.

B. The Birks–Black model fitting

The relative IL intensity reduction as a function of fluence was fitted using the Birks–Black model, which has been extensively used earlier for describing the light yield reduction due to radiation damage in various organic and inorganic scintillators.[45–47] According to this model, the IL intensity change as a function of fluence can be represented as

$$I(\Phi) = \frac{I_0}{1 + k[\exp(\sigma_e \Phi) - 1]}, \tag{4}$$

where $I(\Phi)$ is the NBE IL intensity at fluence Φ, I_0 is the initial NBE IL intensity at zero fluence, σ_e is the effective damage cross section of an individual ion, and k is the ratio between non-radiative and radiative transition rates for the NBE luminescence in the irradiated material.

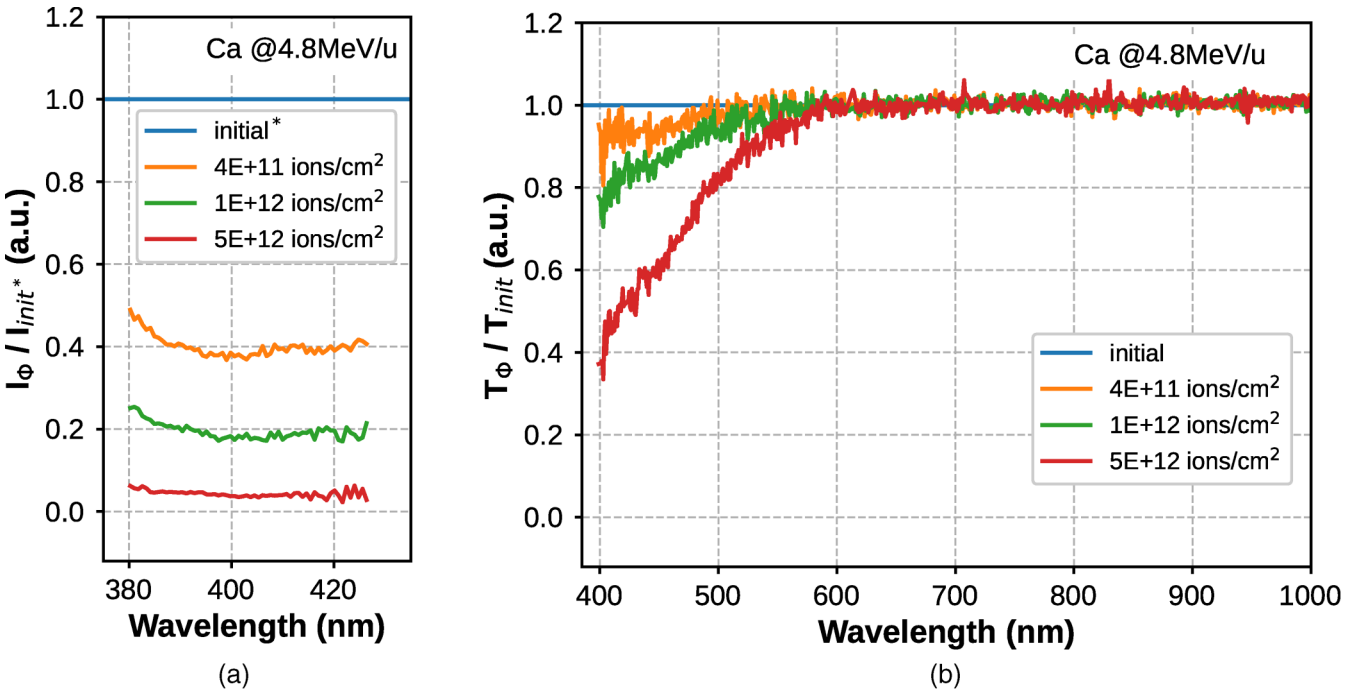

FIG. 6. Relative ionoluminescence intensity I_Φ/I_{init^*} (a) and relative optical transmission T_Φ/T_{init} (b) spectra of ZnO(In) ceramic at various fluences of 4.8 MeV/u ^{48}Ca ion irradiation at 45° beam incidence. Initial IL spectrum corresponds to 6×10^9 Ca − ions/cm^2 fluence.

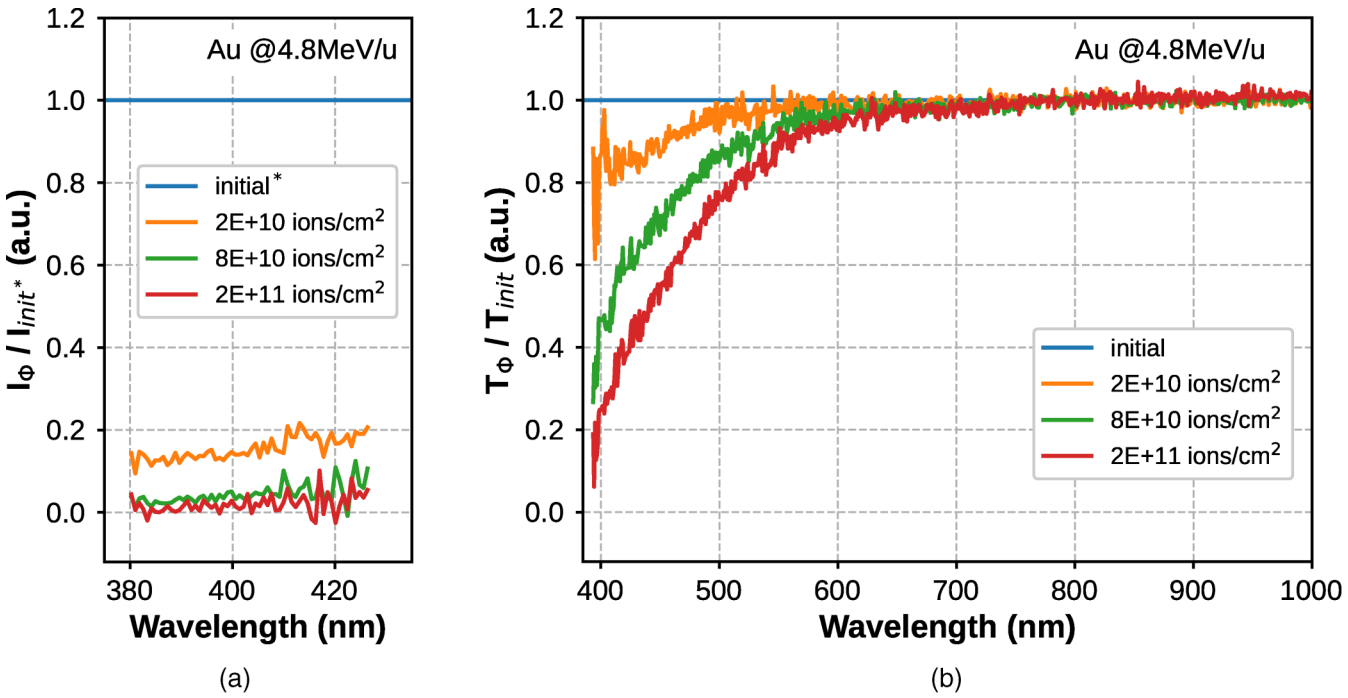

FIG. 7. Relative ionoluminescence intensity I_Φ/I_{init^*} (a) and relative optical transmission T_Φ/T_{init} (b) spectra of ZnO(In) ceramic at various fluences of 4.8 MeV/u ^{197}Au ion irradiation at 45° beam incidence. Initial IL spectrum corresponds to 4×10^8 Au $-$ ions/cm^2 fluence.

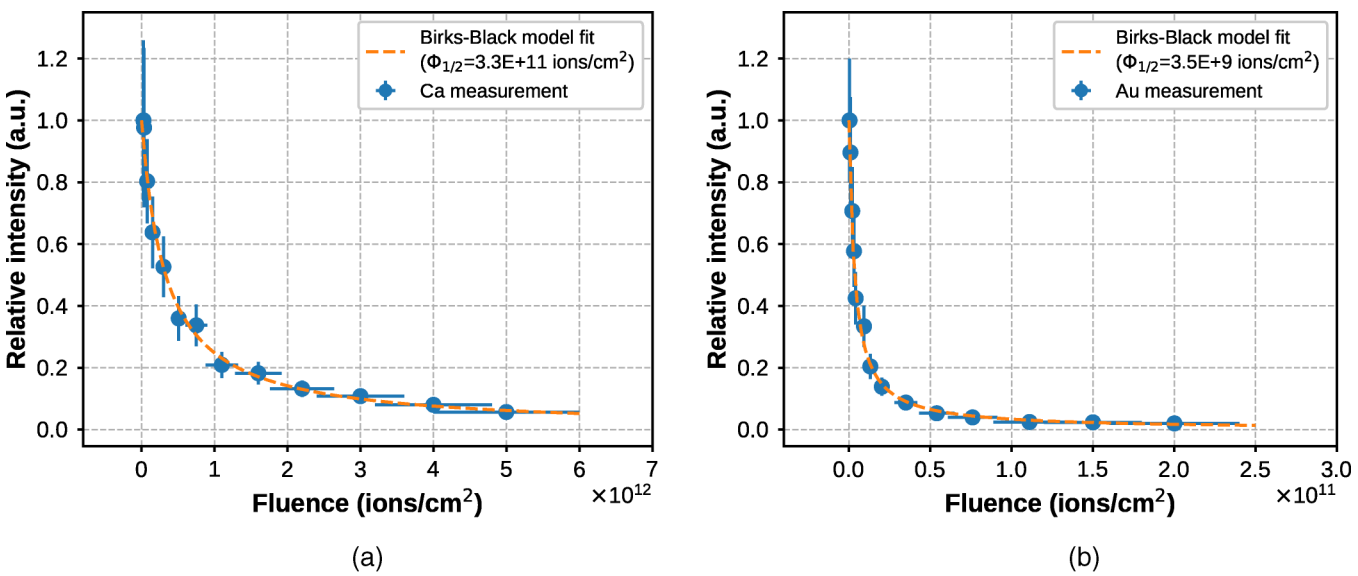

FIG. 8. Relative ionoluminescence peak intensity of ZnO(In) ceramic vs fluence of 4.8 MeV/u ^{48}Ca (a) and ^{197}Au (b) ions. The dashed line shows the Birks–Black model fit using Eq. (5).

TABLE I. Birks–Black model parameter $\Phi_{1/2}$ estimated for ZnO(In) ceramic irradiated with different ions. E_i is the ion incident energy, α is the angle of beam incidence with respect to the sample surface, and S_e and S_n are electronic and nuclear stopping powers calculated by SRIM-2013.

Ion	E_i, MeV/u	α	S_e, keV/nm	S_n, keV/nm	$\Phi_{1/2}$, ions/cm^2
^{48}Ca	4.8	45°	(10–12)[a]	(0.0029–0.022)[a]	$(3.3 \pm 0.7) \times 10^{11}$
^{197}Au	4.8	45°	(37–60)[a]	(0.06–0.48)[a]	$(3.5 \pm 0.7) \times 10^{9}$
^{124}Xe	300	0°	4.2	0.0011	$(2.1 \pm 0.5) \times 10^{12}$
^{238}U	300	0°	11.1	0.0027	$(5.4 \pm 1.2) \times 10^{11}$

[a]The layer thickness from which ionoluminescence signal was generated is unknown. Therefore, possible minimum and maximum energy loss values are presented.

It is important to note that swift heavy ions do not produce one type of defects but a large variety of point defects and defect aggregates. From previous studies of heavy-ion tracks in various materials, e.g., in LiF, it is known that the cross section of single defects is much larger than for defect aggregates.[48] In this work, the parameters k and σ_e are both not associated to any specific defect type. They represent a mixture of different defect species formed along the ion track and their specific contribution to NBE emission cannot be extracted.

The iterative fitting procedure based on the orthogonal distance regression did not converge to a unique solution when Eq. (4) was used to fit the experimental data. An inverse dependency between the free parameter k and σ_e in Eq. (4) led to unlimited number of (k, σ_e) pairs that provide a good fit based on χ^2 test. It was not possible to get stable k and σ_e values output from the fit. Nevertheless, we observed that the product of these two parameters is close to a constant ($k\sigma_e \approx$ const).

We used a simplified Birks–Black model equation, where the exponent is replaced with its first approximation from the Taylor series. The relative IL intensity of damaged vs initial material follows:

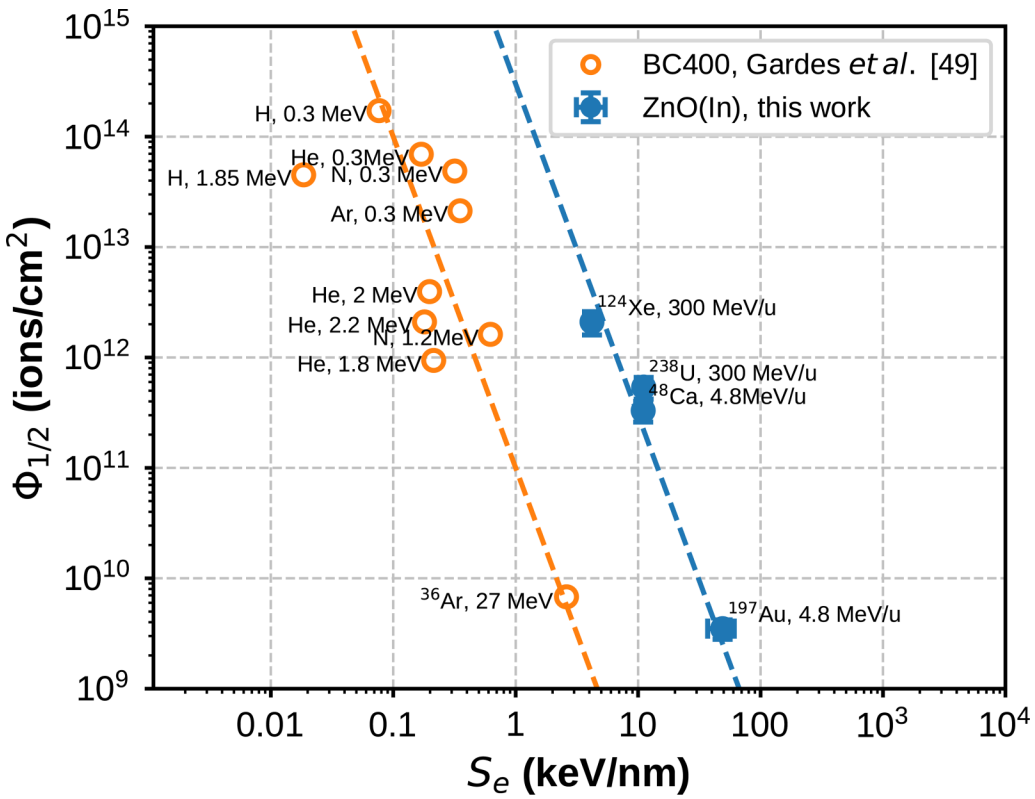

FIG. 9. Critical fluence values, $\Phi_{1/2}$, vs electronic energy loss in the log–log scale presentation. The comparison of previously reported data by Gardès *et al.*[49] for BC400 plastic scintillator (empty orange dots) and ZnO ceramic scintillator data from the present work (filled blue dots). Dashed lines are used to guide the eye.

$$\frac{I(\Phi)}{I_0} = \frac{1}{1+\frac{\Phi}{\Phi_{1/2}}}, \tag{5}$$

where $\Phi_{1/2} = 1/(k\sigma_e)$ is the fluence at which IL intensity is reduced to one-half of the initial intensity (it is also referred to as critical fluence by Gardès *et al.*[49]).

Figure 8 shows the relative IL intensity observed at the NBE peak as a function of Ca and Au ion fluence, together with a fit based on the simplified Birks–Black model [Eq. (5)]. The fit values for the parameter $\Phi_{1/2}$ are presented in Table I together with data obtained based on earlier irradiations with relativistic, 300 MeV/u ^{124}Xe and ^{238}U ions.[7]

Figure 9 shows the ZnO(In) critical fluence values from Table I as a function of the electronic energy loss. The data of the current work are compared to previously reported critical fluences of the BC400 plastic scintillator measured for various ions and energies.[49] There is a clear dependency of the critical fluence $\Phi_{1/2}$ on the electronic energy loss S_e. The critical fluence values become smaller with increasing deposited energy. At a fixed electronic energy loss value, the critical fluence values for ZnO(In) ceramic are orders of magnitude larger than for the BC400 scintillator. This implies that the IL intensity deterioration of ZnO(In) ceramics is orders of magnitude slower than the BC400 plastic scintillator. The slower IL intensity deterioration leads to a longer lifetime during in-beam application as scintillation counter.

V. CONCLUSIONS

Compared to plastic scintillators, ZnO(In) scintillating ceramic irradiated with heavy ions shows excellent tolerance of ionoluminescence properties exhibited under room temperature irradiation, making this material promising for radiation-hard fast scintillation detector application.

The registered ionoluminescence spectra exhibited a single emission band with maximum intensity around 387 nm wavelength. The NBE emission of ZnO matches the maximum photodetection efficiency of a bialkali photo-cathode. Even at the highest fluences, no new emission bands are formed. The ionoluminescence intensity decreases as a function of fluence following the Birks–Black model. The critical fluences (Birks–Black model parameter $\Phi_{1/2}$) were estimated to be $(3.3 \pm 0.7) \times 10^{11}$ and $(3.5 \pm 0.7) \times 10^{9}$ ions/cm^2 for Ca and Au ion irradiation, respectively. These values are several orders of magnitude higher than is known for the BC400 plastic scintillator.

Both Ca and Au ion irradiation causes a yellow-orange coloration of the scintillating ceramic, leading to a transmission loss in the UV and visible light region. Comparing relative IL intensity and relative transmission change as a function of fluence provides a qualitative indication that the loss of the ionoluminescence intensity is more sensitive to the radiation damage induced by Ca and Au ions than the loss of the optical transmission.

ACKNOWLEDGMENTS

DLR funded this research under ERA.Net RUS Plus Project (No. RUS_ST2017-051). The results presented here are based on a UMAT experiment performed in 2020 at the M-branch of the UNILAC at the GSI Helmholtz Center for Heavy Ion Research, Darmstadt (Germany), within the framework of FAIR Phase-0.

AUTHOR DECLARATIONS

Conflict of Interest

The authors have no conflicts to disclose.

Author Contributions

Maxim Saifulin: Data curation (lead); Formal analysis (lead); Investigation (lead); Methodology (equal); Software (lead); Validation (equal); Visualization (lead); Writing – original draft (lead); Writing – review & editing (equal). **Plamen Boutachkov:** Conceptualization (lead); Data curation (supporting); Formal analysis (supporting); Funding acquisition (lead); Methodology (equal); Project administration (lead); Resources (supporting); Supervision (lead); Validation (equal); Visualization (supporting); Writing – original draft (supporting); Writing – review & editing (equal). **Elena Gorokhova:** Resources (equal). **Piotr Rodnyi:** Funding acquisition (supporting); Resources (supporting). **Pascal Simon:** Investigation (supporting); Resources (equal). **Christina Trautmann:** Conceptualization (supporting); Methodology (equal); Resources (supporting); Supervision (supporting); Validation (equal); Writing – review & editing (equal). **Ivan Venevtsev:** Resources (supporting). **Beata Walasek-Höhne:** Resources (supporting); Supervision (supporting); Writing – review & editing (supporting).

DATA AVAILABILITY

The data that support the findings in this study are available from the corresponding author upon reasonable request.

REFERENCES

[1]G. Rosner, "Future facility: FAIR at GSI," Nucl. Phys. B **167**, 77–81 (2007).
[2]P. Forck, T. Hoffmann, and A. Peters, "Detectors for slowly extracted heavy ions at the GSI facility," in *Proceedings of the 3rd European Workshop DIPAC'97* (Frascati, 1997), pp. 165–167.
[3]P. Forck, P. Heeg, and A. Peters, "Intensity measurement of high-energy heavy ions at the GSI facility," AIP Conf. Proc. **390**, 422–429 (1997).
[4]G. Miersch, D. Habs, J. Kenntner, D. Schwalm, and A. Wolf, "Fast scintillators as radiation resistant heavy-ion detectors," Nucl. Instrum. Methods Phys. Res. Sect. A **369**, 277–283 (1996).
[5]K. Kawade, K. Fukatsu, Y. Itow, K. Masuda, T. Murakami, T. Sako, K. Suzuki, T. Suzuki, and K. Taki, "Study of radiation hardness of Gd_2SiO_5 scintillator for heavy ion beam," J. Instrum. **6**, T09004 (2011).
[6]P. Simpson, R. Tjossem, A. Hunt, K. Lynn, and V. Munné, "Superfast timing performance from ZnO scintillators," Nucl. Instrum. Methods Phys. Res. Sect. A **505**, 82–84 (2003).
[7]P. Boutachkov, A. Reiter, B. Walasek-Höhne, M. Saifulin, E. I. Gorokhova, P. A. Rodnyi, and I. Venevtsev, "Radiation hardness investigation of zinc oxide fast scintillators with relativistic heavy ion beams," in *Proceedings of IBIC'19*, (JACoW Publishing, Malmö, 2019), pp. 71–73.
[8]W. Lehmann, "Edge emission of n-type conducting ZnO and CdS," Solid-State Electron. **9**, 1107–1110 (1966).
[9]D. Luckey, "A fast inorganic scintillator," Nucl. Instrum. Methods **62**, 119–120 (1968).
[10]M. Willander, O. Nur, J. R. Sadaf, M. I. Qadir, S. Zaman, A. Zainelabdin, N. Bano, and I. Hussain, "Luminescence from zinc oxide nanostructures and polymers and their hybrid devices," Materials **3**, 2643–2667 (2010).

[11]T. Batsch, B. Bengtson, and M. Moszyński, "Timing properties of a ZnO (Ga) scintillator (NE843)," Nucl. Instrum. Methods **125**, 443–446 (1975).
[12]E. Bourret-Courchesne, S. Derenzo, and M. Weber, "Development of ZnO:Ga as an ultra-fast scintillator," Nucl. Instrum. Methods Phys. Res. Sect. A **601**, 358–363 (2009).
[13]T. Yanagida, Y. Fujimoto, A. Yoshikawa, Y. Yokota, M. Miyamoto, H. Sekiwa, J. Kobayashi, T. Tokutake, K. Kamada, and S. Maeo, "Scintillation properties of in doped ZnO with different in concentrations," IEEE Trans. Nucl. Sci. **57**, 1325–1328 (2010).
[14]E. Gorokhova, S. Eron'ko, A. Kul'kov, E. Oreshchenko, K. Simonova, K. Chernenko, I. Venevtsev, P. Rodnyĭ, K. Lott, and H. Wieczorek, "Development and study of ZnO:In optical scintillation ceramic," J. Opt. Technol. **82**, 837–842 (2015).
[15]K. A. Chernenko, E. I. Gorokhova, S. B. Eron'ko, A. V. Sandulenko, I. D. Venevtsev, H. Wieczorek, and P. A. Rodnyi, "Structural, optical, and luminescent properties of ZnO:Ga and ZnO:In ceramics," IEEE Trans. Nucl. Sci. **65**, 2196–2202 (2018).
[16]F. Muktupavela, J. Maniks, L. Grigorjeva, R. Zabels, P. Rodnyi, and E. Gorokhova, "Effect of in doping on the ZnO powders morphology and microstructure evolution of ZnO: In ceramics as a material for scintillators," Latv. J. Phys. Tech. Sci. **55**, 35–42 (2018).
[17]E. I. Gorokhova, S. B. Eron'ko, E. Oreshchenko, A. V. Sandulenko, P. Rodnyĭ, K. A. Chernenko, I. D. Venevtsev, A. M. Kul'kov, F. Muktepavela, and P. Boutachkov, "Structural, optical, and luminescence properties of ZnO:Ga optical scintillation ceramic," J. Opt. Technol. **85**, 729–737 (2018).
[18]A. Hassan, M. F. Iqbal, S. Maksym, M. Tetiana, M. Azam, Z. Kanwal, I. Irfan, B. Li, and Y. Jiang, "Near-band-edge emission enhancement and suppression of the deep levels in Ga-doped ZnO via surface plasmon-exciton coupling without a dielectric spacer," J. Mater. Sci.: Mater. Electron. **30**, 20544–20550 (2019).
[19]P. Rodnyi, I. Venevtsev, E. Gorokhova, S. Eron'ko, P. Boutachkov, and M. Saifulin, "Fast, efficient, and radiation hard ZnO: In ceramic scintillator," in *Proceedings of the IEEE'19 International Conference, EExPolytech* (IEEE, 2019), pp. 197–200.
[20]D. Millers, L. Grigorjeva, A. Zolotarjovs, F. Muktepavela, J. Grube, A. Spustaka, P. Rodnyi, I. Venevtsev, and E. Gorokhova, "ZnO and ZnO:Ga ceramics for advanced scintillators," Adv. Mater. **9**, 94 (2020).
[21]J. S. Neal, N. C. Giles, X. Yang, R. A. Wall, K. B. Ucer, R. T. Williams, D. J. Wisniewski, L. A. Boatner, V. Rengarajan, J. Nause, and B. Nemeth, "Evaluation of melt-grown, ZnO single crystals for use as alpha-particle detectors," IEEE Trans. Nucl. Sci. **55**, 1397–1403 (2008).
[22]J. S. Neal, D. M. DeVito, B. L. Armstrong, M. Hong, B. Kesanli, X. Yang, N. C. Giles, J. Y. Howe, J. O. Ramey, D. J. Wisniewski, and M. Wisniewska, "Investigation of ZnO-based polycrystalline ceramic scintillators for use as α-particle detectors," IEEE Trans. Nucl. Sci. **56**, 892–898 (2009).
[23]C. Liang, O. Xiao-Ping, Z. Zhong-Bing, X. Liang-Bin, L. Jin-Liang, Z. Xian-Peng, and L. Lin-Yue, "Experimental study on scintillation efficiency of ZnO: In to proton response," Chin. Phys. C **35**, 1037 (2011).
[24]M. M. R. Zeidan, "Using bulk zinc oxide as a neutron radiation detector," Ph.D. thesis (University of Canterbury, 2015).
[25]Q. Zhang, J. Yan, B. Deng, J. Zhang, J. Lv, X. Wen, and K. Gao, "An ultrafast X-ray scintillating detector made of ZnO(Ga)," J. Instrum. **12**, P12033 (2017).
[26]R. Sahani, C. Kumari, A. Pandya, and A. Dixit, "Efficient alpha radiation detector using low temperature hydrothermally grown ZnO:Ga nanorod scintillator," Sci. Rep. **9**, 1–9 (2019).
[27]D. C. Look, "Progress in ZnO materials and devices," J. Electron. Mater. **35**, 1299–1305 (2006).
[28]K. Koike, T. Aoki, R. Fujimoto, S. Sasa, M. Yano, S.-I. Gonda, R. Ishigami, and K. Kume, "Radiation hardness of single-crystalline zinc oxide films," Phys. Status Solidi C **9**, 1577–1579 (2012).
[29]A. Sarkar, M. Chakrabarti, D. Bhowmick, A. Chakrabarti, S. Ray, D. Rafaja, and D. Sanyal, "Defects in 6 MeV H^+ irradiated hydrothermal ZnO single crystal," J. Phys.: Condens. Matter **25**, 385501 (2013).
[30]S. Pal, A. Sarkar, S. Chattopadhyay, M. Chakrabarti, D. Sanyal, P. Kumar, D. Kanjilal, T. Rakshit, S. Ray, and D. Jana, "Defects in 700 keV oxygen ion irradiated ZnO," Nucl. Instrum. Methods Phys. Res. Sect. B **311**, 20–26 (2013).
[31]Y. Song, S. Zhang, C. Zhang, Y. Yang, and K. Lv, "Raman spectra and microstructure of zinc oxide irradiated with swift heavy ion," Crystals **9**, 395 (2019).
[32]D. R. Kumar, K. Ranjith, L. Nivedita, K. Asokan, and R. R. Kumar, "Swift heavy ion induced effects on structural, optical and photo-catalytic properties of Ag irradiated vertically aligned ZnO nanorod arrays," Nucl. Instrum. Methods Phys. Res. Sect. B **450**, 95–99 (2019).
[33]P. Das, R. Biswal, H. Rath, D. Kabiraj, S. Khan, R. Meena, V. Sathe, N. Mishra, and P. Mallick, "Effect of 120 MeV Ag ion irradiation on the structural and electrical properties of NiO/ZnO heterojunction," Mater. Res. Express **6**, 126449 (2020).
[34]N. Kato and M. Sugiyama, "Proton irradiation effects on NiO/ZnO visible-light-transparent solar cells for space applications," Jpn. J. Appl. Phys. **60**, 048001 (2021).
[35]H. Gupta, J. Singh, R. Dutt, S. Ojha, S. Kar, R. Kumar, V. Reddy, and F. Singh, "Defect-induced photoluminescence from gallium-doped zinc oxide thin films: Influence of doping and energetic ion irradiation," Phys. Chem. Chem. Phys. **21**, 15019–15029 (2019).
[36]R. Singh, H. Gupta, R. Mehra, and F. Singh, "Tuning of defects induced visible photoluminescence by swift heavy ion irradiation and thermal annealing in zinc oxide films," Radiat. Phys. Chem. **183**, 109400 (2021).
[37]W. Barth, L. Dahl, J. Glatz, L. Groening, S. Richter, and S. Yaramishev, "Achievements of the high current beam performance of the GSI UNILAC," in *Proceedings of EPAC'04* (JACoW Publishing, Luzern, 2004).
[38]J. F. Ziegler, M. D. Ziegler, and J. P. Biersack, "SRIM—The stopping and range of ions in matter (2010)," Nucl. Instrum. Methods Phys. Res. Sect. B **268**, 1818–1823 (2010).
[39]E. Lamour, P. D. Fainstein, M. Galassi, C. Prigent, C. Ramirez, R. D. Rivarola, J.-P. Rozet, M. Trassinelli, and D. Vernhet, "Extension of charge-state-distribution calculations for ion-solid collisions towards low velocities and many-electron ions," Phys. Rev. A: At. Mol. Opt. Phys. **92**, 042703 (2015).
[40]S. Chattopadhyay, S. Dutta, P. Pandit, D. Jana, S. Chattopadhyay, A. Sarkar, P. Kumar, D. Kanjilal, D. Mishra, and S. Ray, "Optical property modification of ZnO: Effect of 1.2 MeV Ar irradiation," Phys. Status Solidi C **8**, 512–515 (2011).
[41]L. Kappers, O. Gilliam, S. Evans, L. Halliburton, and N. Giles, "EPR and optical study of oxygen and zinc vacancies in electron-irradiated ZnO," Nucl. Instrum. Methods Phys. Res. Sect. B **266**, 2953–2957 (2008).
[42]W. Anwand, G. Brauer, R. Grynszpan, T. Cowan, D. Schulz, D. Klimm, J. Čižek, J. Kuriplach, I. Procházka, C. Ling, A. B. Djurišić, V. Klemm, G. Schreiber, and D. Rafaja, "Characterization of microstructural defects in melt grown ZnO single crystals," J. Appl. Phys. **109**, 063516 (2011).
[43]W. Vehse, W. Sibley, F. Keller, and Y. Chen, "Radiation damage in ZnO single crystals," Phys. Rev. **167**, 828 (1968).
[44]X. Wang, S. He, D. Yang, and P. Gu, "Space radiation damage in ZnO induced by subthreshold electrons: Defect identity and optical degradation," Radiat. Res. **176**, 264–268 (2011).
[45]J. Birks and F. Black, "Deterioration of anthracene under α-particle irradiation," Proc. Phys. Soc. London Sect. A **64**, 511 (1951).
[46]C. Manfredotti, S. Calusi, A. L. Giudice, L. Giuntini, M. Massi, P. Olivero, and A. Re, "Luminescence centers in proton irradiated single crystal CVD diamond," Diamond Relat. Mater. **19**, 854–860 (2010).
[47]P. Sullivan and R. Baragiola, "Ion beam induced luminescence in natural diamond," J. Appl. Phys. **76**, 4847–4852 (1994).
[48]C. Trautmann, M. Toulemonde, K. Schwartz, J. Costantini, and A. Müller, "Damage structure in the ionic crystal LiF irradiated with swift heavy ions," Nucl. Instrum. Methods Phys. Res. Sect. B **164**, 365–376 (2000).
[49]E. Gardès, E. Balanzat, B. Ban-d'Etat, A. Cassimi, F. Durantel, C. Grygiel, T. Madi, I. Monnet, J.-M. Ramillon, F. Ropars, and H. Lebius, "SPORT: A new sub-nanosecond time-resolved instrument to study swift heavy ion-beam induced luminescence—Application to luminescence degradation of a fast plastic scintillator," Nucl. Instrum. Methods Phys. Res. Sect. B **297**, 39–43 (2013).